Converted phases from sharp 1000 km depth mid-mantle heterogeneity beneath Western Europe

J. Jenkins [a,*], A. Deuss [b], S. Cottaar [a]

[a] Bullard Laboratories, Department of Earth Sciences, Madingley Road, Cambridge, CB3 0EZ, UK
[b] Department of Earth Sciences, Universiteit Utrecht, Utrecht, Netherlands

ARTICLE INFO

ABSTRACT

Until recently, most of the lower mantle was generally considered to be well-mixed with strong heterogeneity restricted to the lowermost several hundred kilometres above the core–mantle boundary, known as the D'' layer. However several recent studies have started to hint at a potential change in Earth's structure at mid-mantle depths beneath the transition zone.

Here we present a continental-wide search of Europe and the North Atlantic for mid-mantle P-to-s wave converted phases. Our data set consists of close to 50,000 high quality receiver functions. These are combined in slowness and depth stacks to identify seismic discontinuities in the range of 800–1400 km depth to determine at which depths and in which tectonic settings these features exist. Receiver functions are computed in different frequency bands to resolve the sharpness of the observed discontinuities. We find most seismic velocity jumps are observed between 975–1050 km depth, localised beneath western Europe and Iceland. The shear wave velocity jumps are roughly 1–2.5% velocity increase with depth occurring over less than 8 km in width. The most robust observations are coincident with areas of active upwelling (under Iceland) and an elongate lateral low velocity anomaly imaged in recent tomographic models which has been interpreted as diverted plume material at depth.

The lack of any suggested phase change in a normal pyrolitic mantle composition at around 1000 km depth indicates the presence of regional chemical heterogeneity within the mid-mantle, potentially caused by diverted plume material. We hypothesise that our observations represent either a phase change within chemically distinct plume material itself, or are caused by small scale chemical heterogeneities entrained within the upwelling plume, either in the form of recycled basaltic material or deep sourced chemically distinct material from LLSVPs.

Our observations, which cannot be directly linked to an area of either active or ancient subduction, along with observations in other hotspot regions, suggest that such mid-mantle seismic features are not unique to subduction zones despite the large number of observations that have previously been made in such settings.

1. Introduction

Recent observations from both seismic tomography (Fukao and Obayashi, 2013; French and Romanowicz, 2015) and global viscosity structure (Rudolph et al., 2015) have begun to hint at a potential change in Earth structure at a depth of 1000 km. Tomographic models show that in some regions subducting slabs pond in the mid-mantle above 1000 km after going through the 660 km discontinuity (e.g. Fukao and Obayashi, 2013). Upwellings also appear to be affected at this depth. The recent tomographic model of French and Romanowicz (2015) shows evidence of broad, slow velocity anomalies in the lower mantle up to approximately 1000 km depth, which they interpret as upwelling plumes which divert, pond and change character around 1000 km depth. Results of viscosity inversions have also indicated that there may be an increase in viscosity at approximately 1000 km depth (Rudolph et al., 2015), which has been hypothesised to be due to a viscosity change in periclase (Marquardt and Miyagi, 2015). Alternatively, it has been suggested that there are dynamical consequences of a density cross-over around this depth in a basalt enriched lower mantle (Ballmer et al., 2015).

Seismic observations of velocity jumps in the mid-mantle have been noted for some time (see overview in Kaneshima, 2016). In particular since the 1990s a wealth of seismic observations,

* Corresponding author.
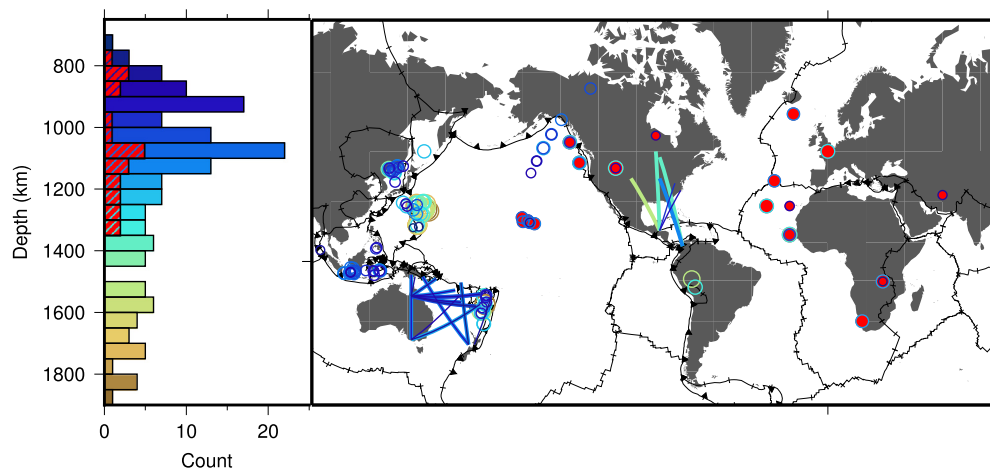 E-mail address: jj405@cam.ac.uk (J. Jenkins).

Fig. 1. The global distribution of previous mid-mantle seismic observations shown both in terms of depth distribution (histogram left) and spatial distribution (map right), with plate boundaries outlined in black. Observations are coloured as a function of depth, and non-subduction related observations (as interpreted in the respective studies), are highlighted in red. Circles represent point observations whereas lines show paths of ScS reverberations where observations are seen along path length. See Supplementary Material section 1 for full dataset and references. (For interpretation of the references to colour in this figure legend, the reader is referred to the web version of this article.)
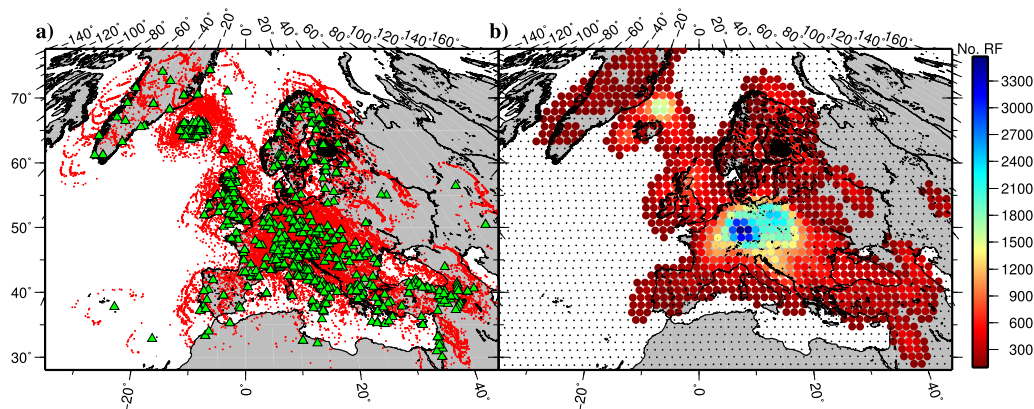

Fig. 2. a) Distribution of 740 seismic stations (green triangles) and 1050 km depth pierce points (red points) for the 49,572 RFs used in this study. **b)** Regional extent of the evenly spaced 2 degree caps used to set up RF stacks, circles represent viable stack regions containing greater than 100 RFs coloured by the number of RFs contained within the stack. (For interpretation of the references to colour in this figure legend, the reader is referred to the web version of this article.)

largely focused on subduction zone regions, have identified signals of potential mid-mantle local seismic discontinuities ranging from 800–2000 km depth. The majority of these observations lie in the range of 850–1200 km depth as shown in Fig. 1. Seismic discontinuities in the deep Earth usually represent phase transitions or compositional layering, either of which could play an important role in whole mantle dynamics.

A range of methods have been used to search for deep seismic observations including: Pds conversions (Shen et al., 2003; Van der Meijde et al., 2005; Deuss et al., 2013), SKSds conversions (Vinnik et al., 2010), P′P′ precursors (Le Stunff et al., 1995), SS precursors (Deuss and Woodhouse, 2002; An et al., 2007; Deuss, 2009; Gu et al., 2009), PP precursors (Deuss, 2009), off great-circle-path scattered precursory PP energy (Rost et al., 2008) and ScS reverberations (Courtier and Revenaugh, 2008). The majority of studies use near source SdP conversions (e.g. Kawakatsu et al., 1994; Kaneshima and Helffrich, 1999; Vinnik et al., 2001; Castle and Van Der Hilst, 2003; Vanacore et al., 2006; Yang and He, 2015). SdP conversions require large magnitude, deep sourced earthquakes, which may explain why most lower mantle reflectors have previously been found in subduction zone regions, see Fig. 1. However a small number of studies have found evidence of such signals in non-subduction regions. These include several observations related to areas of active upwelling: Iceland and Hawaii (Shen et al., 2003), southern Africa (Le Stunff et al., 1995), and other hotspot regions

(Gu et al., 2009). A few observations are associated with tectonically stable regions: NW Europe and the southern tip of Africa (Vinnik et al., 2010), Asia (Deuss, 2009) and Canada (Deuss et al., 2013).

In this study we focus on Europe and the North-Atlantic region, searching for mid-mantle seismic observations on a continental scale using P-to-s converted phases or receiver functions. This area provides an excellent natural laboratory, with its dense instrumentation and range of tectonic settings: active upwelling under Iceland, stable cratonic regions in Greenland and Central Europe, as well as ancient and currently active subduction zones in the Mediterranean.

2. Data and method

2.1. Receiver function dataset

This study combines the dataset across Greenland and Iceland from Jenkins et al. (2016) and the dataset across the rest of Europe from Cottaar and Deuss (2016), see Fig. 2 for data coverage. Most of these data are sourced from the IRIS and ORPHEUS data centres by selecting all events of Mw >5.5 within an epicentral distance range of 30–90 degrees from stations, see Supplementary Material section 2 for full list of networks. The coverage in Iceland is supplemented by two additional networks: the University of Cam-
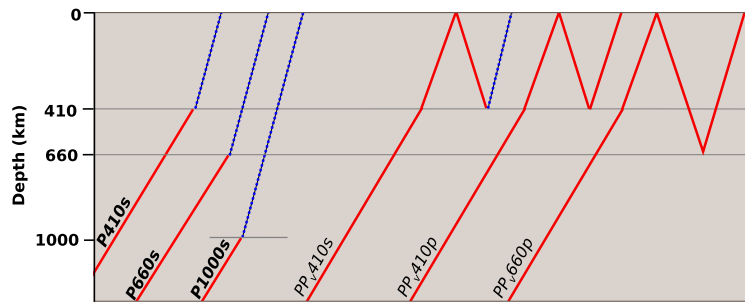
Fig. 3. Ray paths of P-to-s converted phases this study focuses on (labelled in bold italic) and major interfering surface multiples (labelled in italics), where v denotes a topside reflection. P waves are plotted as red solid lines and S waves as dotted blue lines.

bridge Icelandic Seismic Network and the Iceland Meteorological Office network.

P-to-s receiver functions (RFs) are created via a deconvolution of the vertical from the radial components of motion, which highlights P-to-s converted phases generated by seismic discontinuities beneath the recording station. These converted waves, which are referred to as Pds phases (where d denotes depth of conversion), appear as delayed arrivals after the direct P wave. We pre-filter the data between 0.01 and 0.2 Hz and build RFs using a Gaussian pulse of 0.4 using the iterative time domain method of Ligorría and Ammon (1999). The original dataset comprises of over 500,000 RFs. After both automated and manual quality controls (see Cottaar and Deuss, 2016 and Jenkins et al., 2016 for details), we are left with a dataset containing over 49,500 high quality RFs, the distribution of which is shown in Fig. 2a. While Cottaar and Deuss (2016) manually remove stations where multiples interfere with the P410s arrival, here we include these data as we focus on observations from greater depths. Synthetic RFs are obtained by computing synthetic seismograms with the reflectivity method of Fuchs and Müller (1971) and following the same RF procedure used for real data.

2.2. Method overview

Pds phases (shown in Fig. 3), have a small amplitude and are difficult to observe above noise in individual RF traces. Thus RFs are generally combined in stacks to enhance coherent signals and reduce incoherent noise. In Jenkins et al. (2016) and Cottaar and Deuss (2016), a common conversion point (CCP) stack is used to combine the RFs and analyse the mantle transition zone topography. One downside of CCP stacks is that it is difficult to interpret observed arrivals at other depths than the main seismic discontinuities around 410 and 660 km depth, as one cannot distinguish from the CCP stack if they are converted phases from the observed depth, or multiples from shallower depths. Here we turn to slowness stacks to confirm true observations of mid-mantle seismic conversions using the following approach:

1. We use 8457 points, spaced equally every 2 degrees (Rakhmanov et al., 1994), across Europe to build stacks including RFs for which the 1050 km depth pierce points fall within a circular cap of 2 degree radius. The caps allow overlap of RFs between adjacent stacks. Caps containing a minimum of 100 RFs are used to make stacks, giving us a total of almost 1000 stacks across the area of study (Fig. 2b).
2. For each cap RFs are stacked in both the slowness-time and depth domain. We use the slowness-time stacks to confirm if an arrival is indeed a converted phase coming from depth. The time-to-depth converted stacks are used to determine the depth from which the converted phases originate. See details in Section 2.3.

3. We use an automated procedure to identify conversions from the mid-mantle and suggest a quality of the observations. Quality categorisations are manually checked and potentially downgraded depending on the overall quality of the stack. See details in Section 2.3.
4. For regions where we find consistent high-quality conversions from mid-mantle depths, we combine multiple caps to produce higher quality stacks of these observations. We use the regional dataset to reproduce RFs in different frequency bands to test the frequency sensitivity of the converted phases and thus the width of the seismic discontinuity. See details in Section 2.4.

2.3. Depth and slowness-time stacks

Slowness stacks (also known as vespagrams), identify coherent signals in the time-slowness domain. We stack RFs by groups of nearby pierce points at 1050 km depth. We shift RF traces to a reference epicentral distance for a range of linear move-outs (assuming a constant slowness with epicentral distance). For each potential move-out we create a vespagram trace (VT) by summing all shifted traces together, as shown in equation 1.

$$\text{VT}(s_j) = \frac{1}{N} \sum_{i=1}^{N} RF_i(t + s_j(\Delta_{RF_i} - \Delta_{REF})) \qquad (1)$$

Where s_j refers to a specific differential slowness with respect to the direct P wave, t is time referenced to the P wave arrival, Δ_{REF} denotes the chosen reference epicentral distance, Δ_{RF_i} is the station event epicentral distance for RF_i and N is the number of stacked traces. We generally use a reference epicentral distance of 65 degrees, but use 75 degrees for several regional stacks with data mostly from more distal epicentral distances. Individual vespagram traces for a range of move-outs or slownesses are combined to form slowness stacks.

Slowness stacks provide a useful tool for discriminating between true Pds arrivals and multiples, which may arrive at times similar to converted phases, but with a different slowness (see Supplementary Material section 3, major interfering phase ray paths are shown in Fig. 3). Pds conversions have a steeper incoming angle than the direct P phase, and thus always stack most coherently at negative slowness' relative to P. Conversely multiples have a shallower incoming angle and a corresponding positive relative slowness, as shown for synthetics in Fig. 4a and b.

Depth stacks are created by transforming each individual trace from time to depth before being summed together. It is important to account for 3D velocity variations, especially beneath Iceland, where velocities at 150 km can be up to 11% slower than reference 1D models (Rickers et al., 2013). Without accounting for velocity corrections across the mantle beneath Iceland a conversion from 1000 km depth would appear to come from ∼1050 km
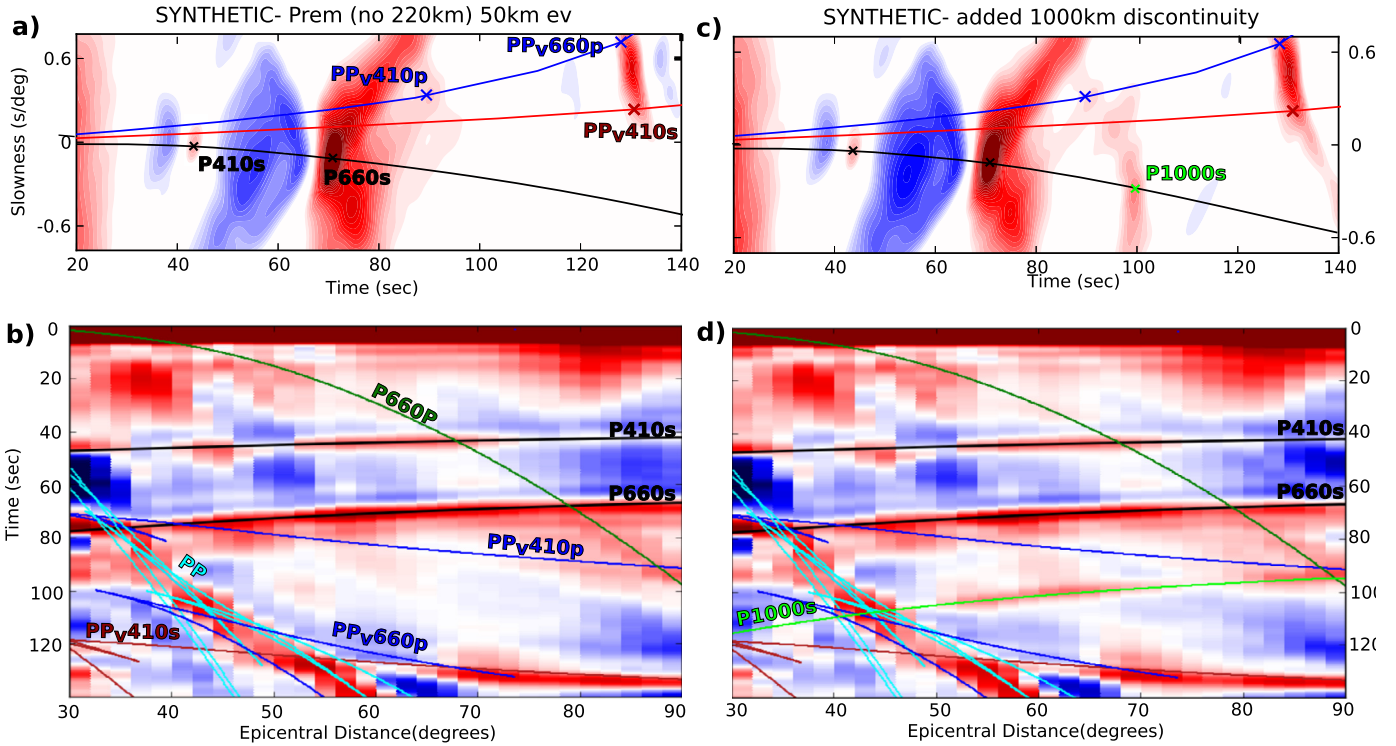
Fig. 4. a) Example of a synthetic slowness stack computed PREM without the 220 km discontinuity (Dziewonski and Anderson, 1981). Cross marks show arrivals associated with the major discontinuities at 410 km and 660 km depth as labelled. The black line shows the time-slowness relationship for P-to-s converted phases, while blue and red lines show predicted positive slowness' for S and P surface bounce multiples. **b**) Epicentral distance stack of same synthetic data highlighting major phases as labelled. Right hand panels **c**) and **d**) show the same but with a 1.5% jump added to the velocity model at 1000 km depth, showing the phases associated with that discontinuity. (For interpretation of the references to colour in this figure legend, the reader is referred to the web version of this article.)

depth (see supplementary Fig. S5). The RFs across Iceland and Greenland, are converted to depth using a tomographic shear wave velocity model, down to 1400 km, of the North-Atlantic region (Rickers et al., 2013). We use a depth dependent scaling factor to calculate P-wave velocity variations based on that proposed for S40RTS (Ritsema et al., 2011). The RFs across the rest of Europe are converted to depth using the recent model EU60 (Zhu et al., 2015), which includes both S and P velocities down to 1100 km depth. PREM (Dziewonski and Anderson, 1981) is used for depths below 1100 km. The standard error is calculated for both depth and slowness stacks, allowing identification of robust signals, which we consider as peaks showing >2 standard error (SE). Accordingly only signals above 2 SE are shown in slowness stacks (in 2D time-slowness space), while 1D depth stacks show true amplitude with errors.

Each pair of slowness/depth stacks is given a quality categorisation, as to whether or not it contains a clear mid-mantle signal. This is initially carried out using an automated algorithm in an attempt to quantitatively define quality categories. Quality criteria are based on: 1) if the P660s peak is clearly observable and at the correct predicted slowness, 2) whether or not there is a peak observed above 2 SE in the depth stack between 800–1400 km depth, and 3) a determination of how close the slowness of that peak is to the predicted Pds slowness. The five quality categories are defined as: "good", "maybe", "anomalous slowness", "null" or "poor". Examples of stacks classified as each of these categories as well as further information about the quality classification system is shown in the Supplementary Material section 4.

Finally stack classifications are manually inspected and potentially downgraded. This step is used to check for issues such as streaks in the stacks caused by a concentration in data from a restricted epicentral distance range. This can lead to uncertainty in the true slowness, as arrivals are smeared across a range of

slowness'. Such issues can be even more problematic for bimodal data distributions where streaks in two directions can interfere to produce artifacts which appear to have "good" arrival characteristics. Stacks are visually inspected for these features and manually downgraded where necessary, see Supplementary Material Figure S3e for an example of streaking in a stack.

2.4. Exploring frequency sensitivity

Converted phases are sensitive to discontinuities equal to or less than half the wavelength of the incoming P wave (Bostock, 1999). For a sharp discontinuity conversions are visible over a range of different frequencies, while for a broad discontinuity conversions become reduced in amplitude at higher frequencies. Thus by investigating data in a range of frequency bands it is possible to put some constraints on the sharpness of causative discontinuities.

For each high quality regional stack we recompute our data in a range of different frequency bands. Data are bandpass filtered with a constant minimum of 0.01 Hz and a maxima varying from 0.2 to 0.7 Hz, with RFs then created using Gaussian pulses with a width (a) of half the minimum wavelength or approximately twice the maximum data frequency (see Supplementary Material, section 5).

The Gaussian filter is defined as: $G(\omega) = e^{\frac{-\omega^2}{4a^2}}$ where ω is radial frequency and a is filter width.

Using the stacks in the depth domain, corrected for 3D velocity variations, we analyse the resulting amplitudes of mid-mantle converted arrivals across the different frequency bands and compare these to the behaviour of P410s and P660s (van der Meijde et al., 2003; Schmandt, 2012). For comparison, we compute synthetic seismograms for velocity jumps in the mid-mantle using reflectivity synthetics (Fuchs and Müller, 1971) and process and stack them in different frequency bands similar to the observations.
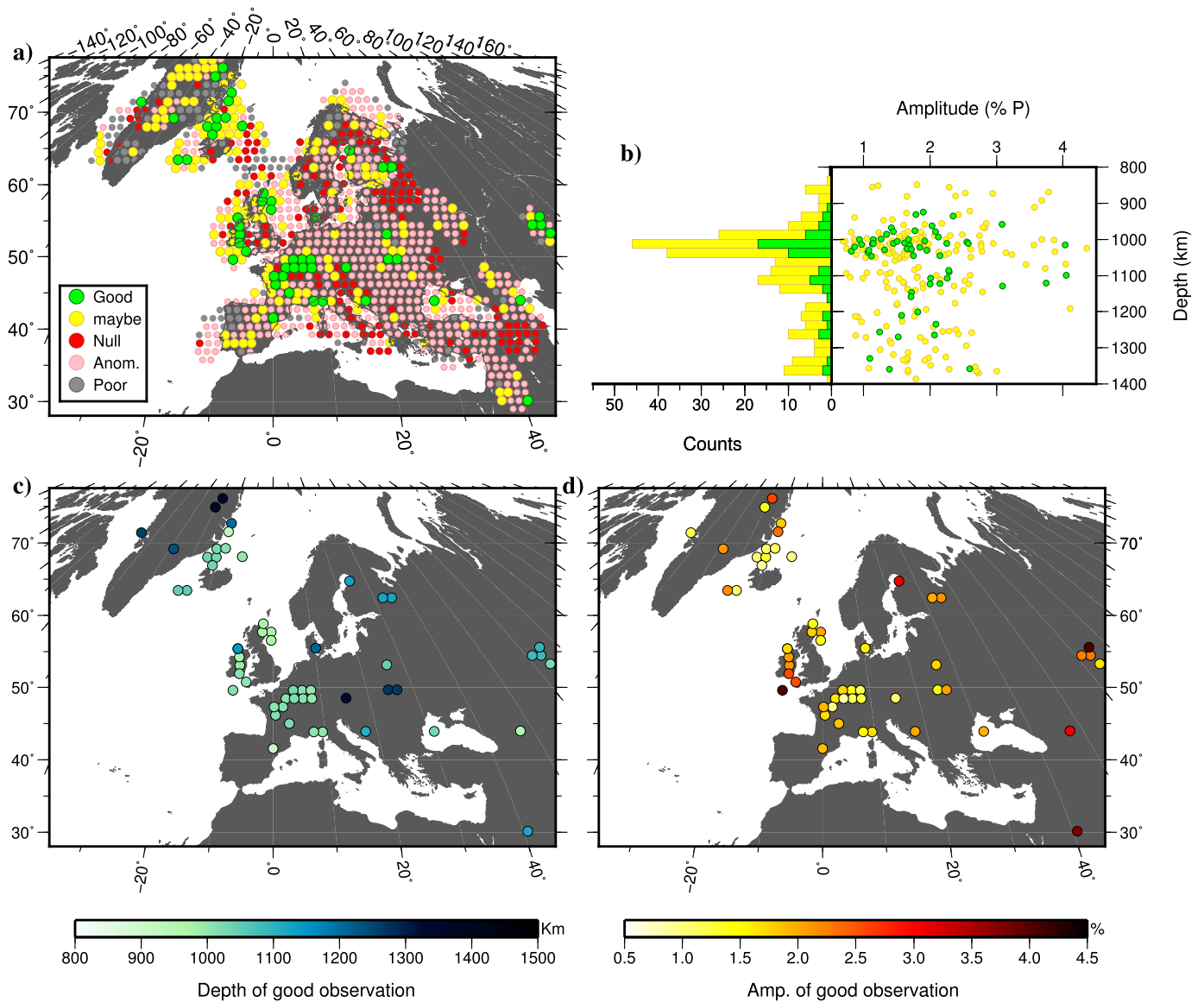
Fig. 5. a) RF stack regions coloured by assigned quality of mid-mantle observations, **b**) graph and stacked histogram showing amplitude and depth distribution of all good (green) and maybe (yellow) observations, **c**) depth variation of all "good" observations, **d**) amplitude variation of all "good" observations. (For interpretation of the references to colour in this figure legend, the reader is referred to the web version of this article.)

3. Results

3.1. Observations of mid-mantle seismic discontinuities

The mid-mantle observations classified as "good" are marked in green in Fig. 5a. The distribution of results is non-continuous and patchy, though there are several stacks showing "good" or "maybe" observations grouped together in robust regions, e.g.: north of Iceland, NE of Scotland, Ireland and Eifel (Germany/N. France). A handful of stacks are clear examples of "null" observations (shown in red), where there is no energy observed within mid-mantle depth ranges. Most observations have been classified as "anomalous slowness" (shown in pink in Fig. 5a), and energy in these stacks is likely due to surface multiples as shown in the example slowness stack in Fig. 4. These stacks can be thought of as less confident "null" observations.

The depth distribution of observations is shown in Fig. 5b. Potential observations ("maybes") are found throughout the investigated range from 800–1400 km depth, but there is a clear peak at

~1000 km depth. This is supported by the depth distribution of "good" observations (also shown in Fig. 5c), the majority of which show consistent depths around 1000 km.

The amplitude of observations varies from 0.8–4.5% of the direct P wave peak (Fig. 5b and d). Most arrivals show significantly smaller amplitudes than the 410 km depth and 660 km depth transition zone discontinuities which are generally 4% and 7% respectively. We also note that there does not appear to be any correlation between depth and amplitude of observations (Fig. 5b), and no clear lateral variation in amplitude (Fig. 5d). The observed amplitude of a conversion in a stack is affected by multiple factors, including noise level of RFs and how many of the stacked RFs observe the signal. Thus we only take the amplitude range observed as a minimum estimate of the true amplitude of deep converted phases.

Arrivals from depths beneath 1000 km can be seen in the histogram of Fig. 5b. However these signals are often barely above error, inconsistent between adjacent stacks and are less reliable in terms of slowness, which is why they are not further discussed.
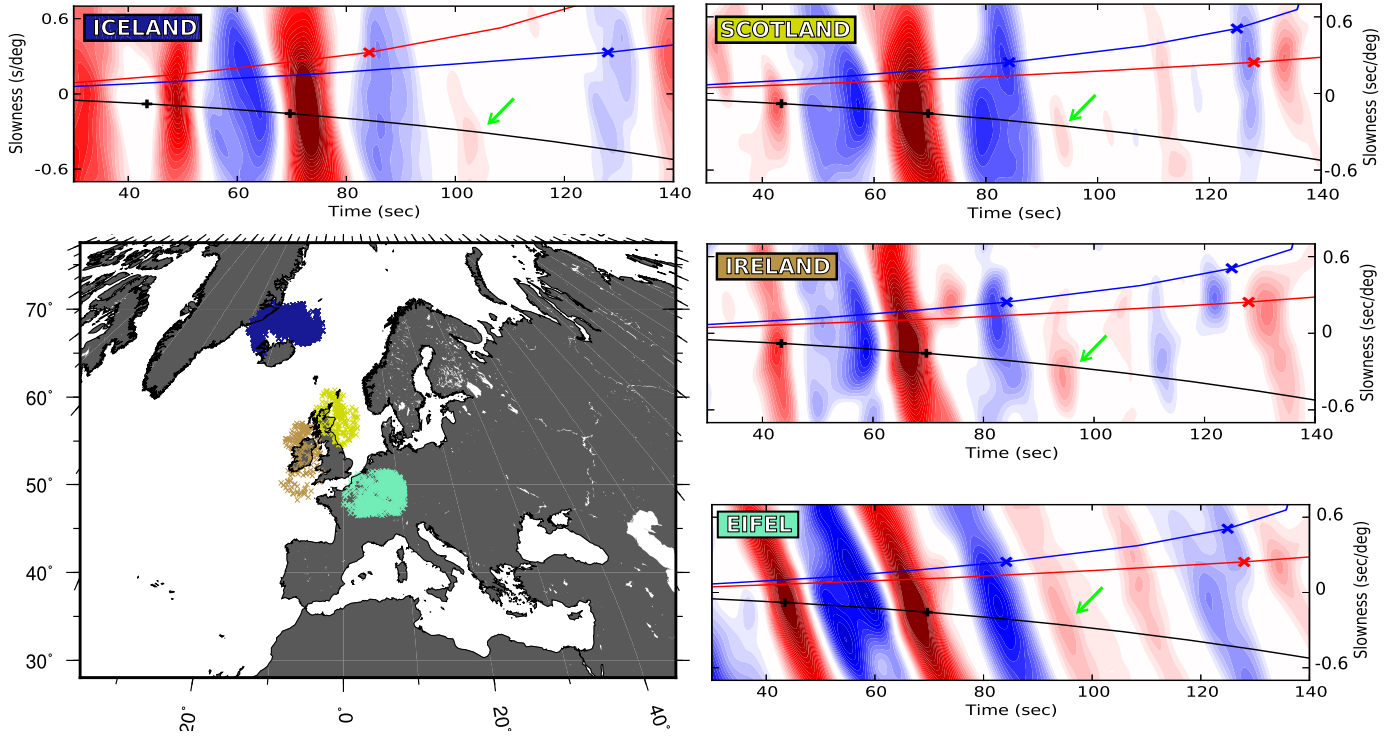
Fig. 6. Regional scale slowness stacks of RFs with consistent conversions from mid-mantle depths (as shown in Fig. 5), in four locations across western Europe. Black curves show the time-slowness relationship for P-to-s converted phases with black crosses denoting P410s and P660s, while blue and red lines show the predicted positive slowness' for the surface bounce multiples PPvdp and PPvds, respectively, with coloured crosses denoting the PPv410p, PPv660p (blue) and PPv410s (red) arrivals. (See also Fig. 4.) The mid-mantle P1000s phase is highlighted by green arrows. The 1050 km pierce points of each group are shown in the central map. (For interpretation of the references to colour in this figure legend, the reader is referred to the web version of this article.)

3.2. Regional stacks

Based on our regional grid of stacks, we identify areas where there are multiple "good" observations and group these together in robust regions (see Fig. 5). These regional stacks all lie in Western Europe following a NW–SE trend from Iceland towards Eifel, with consistent near 1000 km positive arrivals and realistic Pds conversion slowness' (Fig. 6). Epicentral distance stacks, Fig. 7, clearly show this deep arrival appearing at close to 100 s, in events from distal epicentral distances (60–90 degrees). However a lack of data coverage from closer events means it is hard to clearly distinguish the small amplitude arrival at smaller distances, where there is also likely to be interference from PP and PP precursory phases.

3.3. Negative peaks

The results shown in Fig. 5 and discussed thus far are for an analysis conducted on positive amplitude arrivals. A similar analysis was conducted for negative amplitude arrivals. A systematic search of 2 degree cap stacks shows a slight suggestion of arrivals from ~800 km, however the observation of interfering multiples arriving at the same time as these peaks mean observations are often unclear and accordingly there is a lack of clear consistent "good" observations, unlike the 1000 km peak shown in Fig. 5b.

We also note a negative arrival between ~80–85 s is seen in regional stacks, see Fig. 6. This negative energy clearly has a positive slowness and is thus identified as a multiple in the Ireland stack in Fig. 6. However in several stacks, Scotland and Eifel in particular, there also appears to be a negative arrival at realistic Pds slowness at ~80–85 s. The Iceland stack shows some sign of this arrival, but this could simply be due to smearing from the multiple above. The observation of a shallower negative arrival is not directly related to the positive 1000 km arrival as it is not observed consistently in all stacks where the later positive peak is observed.

The presence of a negative multiple with little differential slowness make this negative ~80–85 s arrival far less convincing than the positive peak at ~100 s. Because of the lateral extent and consistency in reliable positive amplitude 1000 km depth observations, we focus on defining their character and interpreting their underlying cause in the remainder of this paper.

3.4. Frequency dependence

We apply frequency dependence analysis to our regional subsets of RFs, the results of which are shown in Fig. 8 (for slowness stacks across all investigated frequencies see Supplementary Material section 7). The amplitudes of the Pds phases show a reduction at higher frequencies for P660s, while P410s and P1000s amplitudes remain stable across the frequency range. The average amplitude reduction for P660s between the highest and lowest frequency stack is 41% indicating a broader transition than the other two discontinuities.

The P1000s peak appears to show little or no amplitude variation in the frequency spectrum investigated. Pds phases are sensitive to velocity jumps with a width of half the wavelength (λ_P) of the incident P wave: $\frac{\lambda_P}{2}$ (Bostock, 1999), thus the observability of P1000s at frequencies up to at least 0.7 Hz (Gaussian width of 1.4), indicates a relatively sharp causative feature. Taking a P wave velocity at 1000 km of ~11.5 km s^{-1}, suggests waves are being converted at a discontinuity which is at most ~8 km wide.

3.5. Frequency dependence – synthetic modelling

Fig. 9 shows the results for the synthetic stacks for shear wave velocity jumps of 2 and 3.2% with discontinuity widths of 0, 20, and 40 km. Jumps in P wave velocity and density in the synthetic models are scaled, but P-to-s conversions are mainly sensitive to
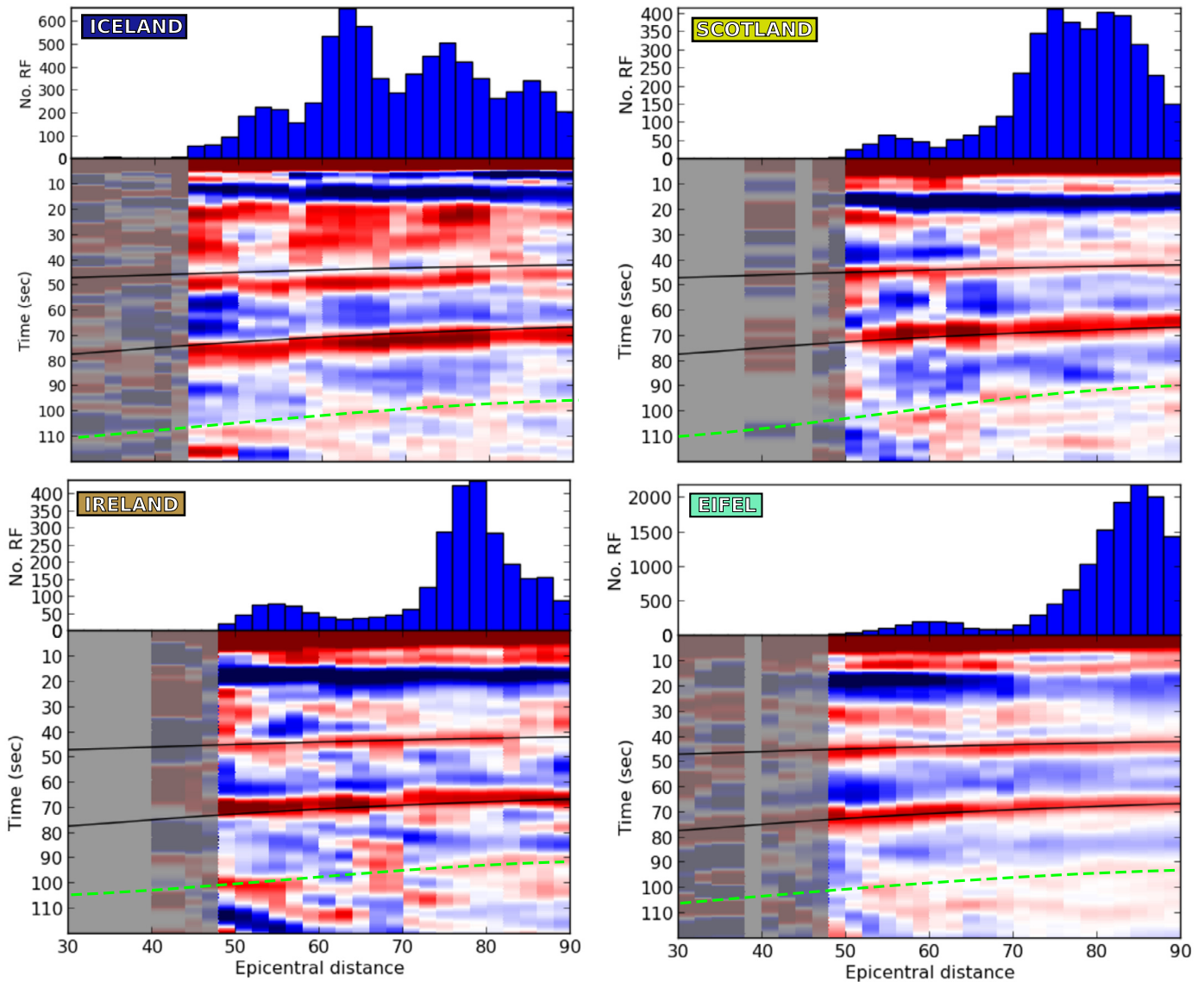
Fig. 7. Regional scale epicentral distance stacks of RFs showing arrivals from mid-mantle depths at approximately 100 s highlighted with green dashed lines. Arrival of major converted phases P410s and P660s are shown as solid black lines. Stack sections containing <15 RFs have been greyed out. Upper panels show the distribution of event RFs going into stacks, where data has been smoothed between 3 adjacent bins.
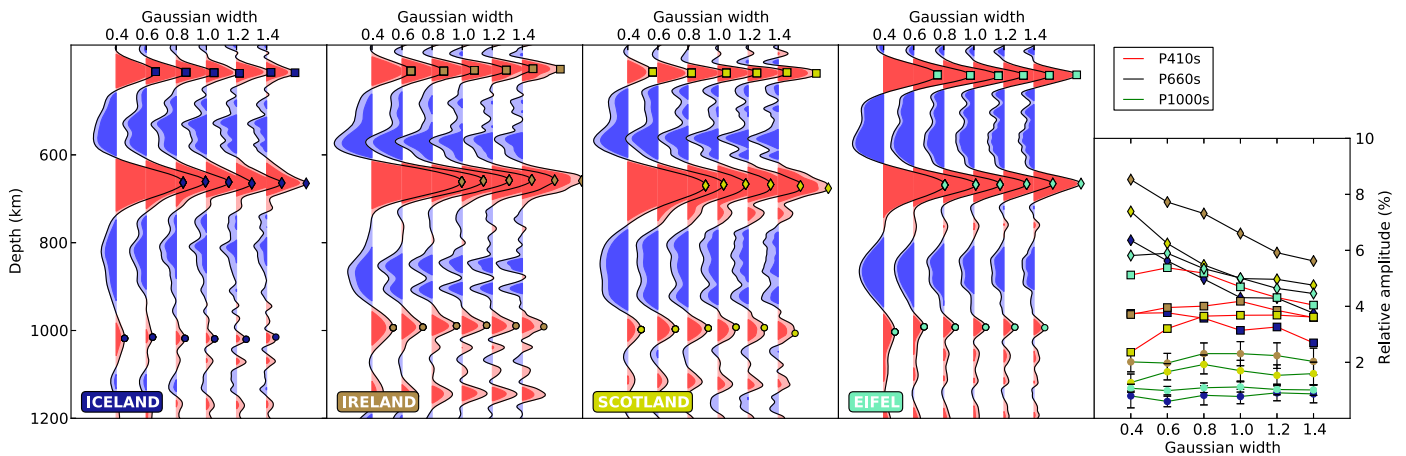

Fig. 8. Waveforms of regional scale RF depth stacks for a range of different frequency bands. The maximum amplitudes of P660s, P410s and P1000s arrivals are plotted on the waveforms as diamonds, squares and circles respectively. The variation of P660s (black lines and diamonds), P410s (red lines and squares) and P1000s (green lines and circles) amplitudes with frequency is shown in the right hand graph, error bars based on ±2 SE are shown for P1000s amplitudes (colour code for the regional stacks is the same as in Fig. 6). (For interpretation of the references to colour in this figure legend, the reader is referred to the web version of this article.)
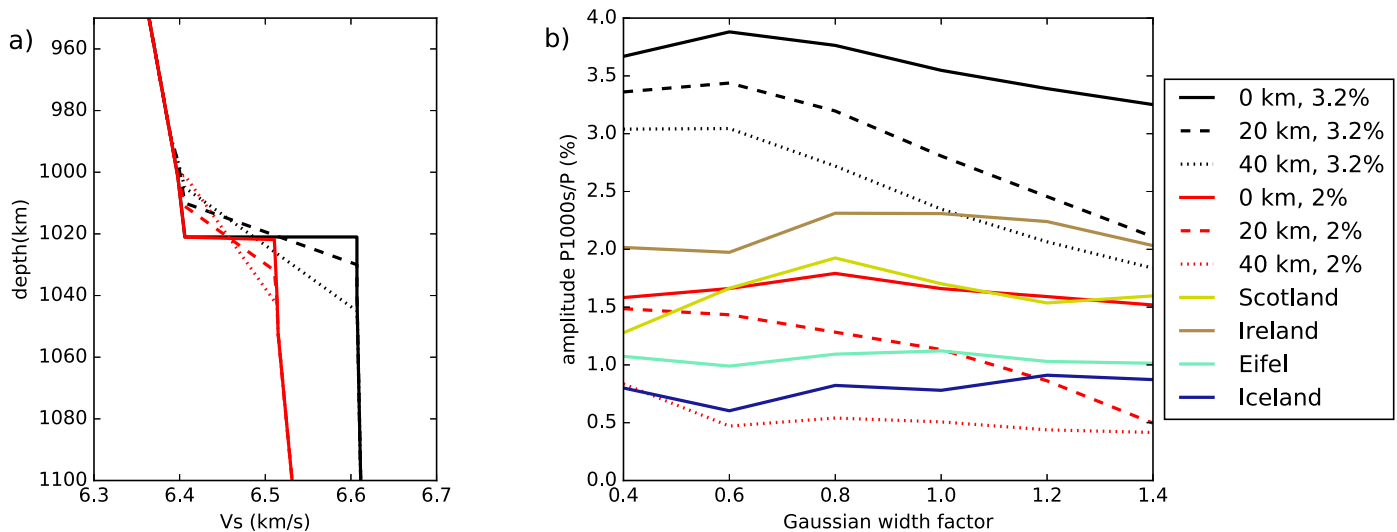
Fig. 9. Amplitude frequency dependence of P1000s arrivals in RF stacks for synthetic cases compared to observed values for the regional stacks. Shear wave velocities for the synthetics are plotted in **a**). The models represent a 3.2% velocity jump with a width of 0 km (blue solid), 20 km (blue dashed) and 40 km (blue dotted), and a 2% velocity jump with a width of 0 km (red solid), 20 km (red dashed) and 40 km (red dotted). The Pds phase amplitude dependence as a function of frequency is shown in **b**) against observations in the regional stacks (colour code for the regional stacks is the same as in Fig. 6). (For interpretation of the references to colour in this figure legend, the reader is referred to the web version of this article.)

the shear wave velocity jump. We exclude models with a negative velocity jump, or with a thin layer of anomalous velocities, as both these cases cause a polarity reversal in the P1000s arrival which we do not see in our observed stacks. Synthetic results are then compared to the amplitude variations with frequency in the regional stacks.

The models for a velocity jump of 3.2% (black lines in Fig. 9) show a strong decrease in amplitude for broader transitions (dotted black lines in Fig. 9), which is particularly noticeable at high frequencies. For the models with a 2% velocity jump (red lines in Fig. 9), this trend breaks down for the 40 km wide case (dotted red lines in Fig. 9). In this last case, at the higher frequency end two separate arrivals are observed related to the second-order discontinuity at the top and the bottom of the transition, while the main arrival disappears (see full synthetic stacks in Supplementary Material section 8). We find that observations in the regional stacks with a single positive arrival beneath Scotland, Ireland and Eifel, fit best with a discontinuity of zero-width or a discontinuity of less than 20 km wide. The observations beneath Iceland could relate to multiple smaller closely spaced first and second-order discontinuities.

When comparing amplitudes, we see the regional stacks suggest relative amplitudes between 0.8–2.0% velocity jump, related to shear wave velocity jumps of ∼1.0–2.5%. We should emphasise that these are minimum estimates, as our stacks are over a wide region. Broad stacks can include some data which do not sense a small scale localised velocity jump, additionally any topography on the discontinuity or mis-corrections for lateral velocity variations will lead to incoherent stacking and thus smaller amplitudes. Indeed, the two-degree cap stacks in Fig. 5d, observe relative amplitudes of up to 4.5%. Any physical explanation for these scatterers around 1000 km should be able to account for a sharp positive transition of at least several percent.

4. Discussion

We observe regional, sharp, positive velocity jumps of several percent around 1000 km beneath Western Europe. Here we will discuss these observations in terms of previous observations (4.1), their relationship to tomographic models (4.2), and potential explanations (4.3).

4.1. Comparison to previous observations

The depth distribution of our observations in Fig. 5b is dominated by a peak at ∼1000 km depth which is roughly consistent with the peak at ∼1025–1050 km depth observed in the depth distribution of previously published observations shown in the histogram of Fig. 1. We do not observe the shallower global peak present at 850–900 km depth in Fig. 1, but note that this occurs at a depth we have identified as likely to contain interfering surface multiples in our dataset, as shown in Fig. 4. We also note that while both histograms agree on an increased number of arrivals occurring around 1000 km, direct comparison is difficult. The histogram of previously published results is biased by studies in subduction zone regions, multiple studies in the same area and contains different body wave data with different sensitivities to deeper discontinuities. In contrast, the histogram from our study is more statistically significant as it represents equal-area spaced robust observations across one continent using one data type, with bias only resulting from data coverage.

Previous observations of mid-mantle seismic signals have been reported in locations where we also see arrivals: near Iceland (Shen et al., 2003) and in southern Britain (Vinnik et al., 2010). The depths of their observations are not consistent with ours. Shen et al. (2003) observe converted Pds arrivals to the south of Iceland, at a depth of 1120 ± 20 km. With thirteen years more data, we observe Pds arrivals from 1030 km depth both north and west of the island. Vinnik et al. (2010) observe mid-mantle converted SKSp arrivals in similar locations to our study but at greater depths – 1240–1270 ± 10 km across a large region of southern Britain and NW Germany/France. We see some suggestions of this arrivals in the Eifel regional stack at ∼1204 km depth, but it is smeared across a range of slownesses making it difficult to determine whether it is a true arrival or a multiple. However the study of Vinnik et al. (2010) shows little suggestion of a P1000s arrival in this region which is the much clearer arrival in our study. We hypothesise that the wider sampling regions, lack of 3D velocity corrections and lower frequency content of seismic arrivals used in previous studies compared to the current study, means that the 1000 km depth arrivals we observe may have previously been averaged out.
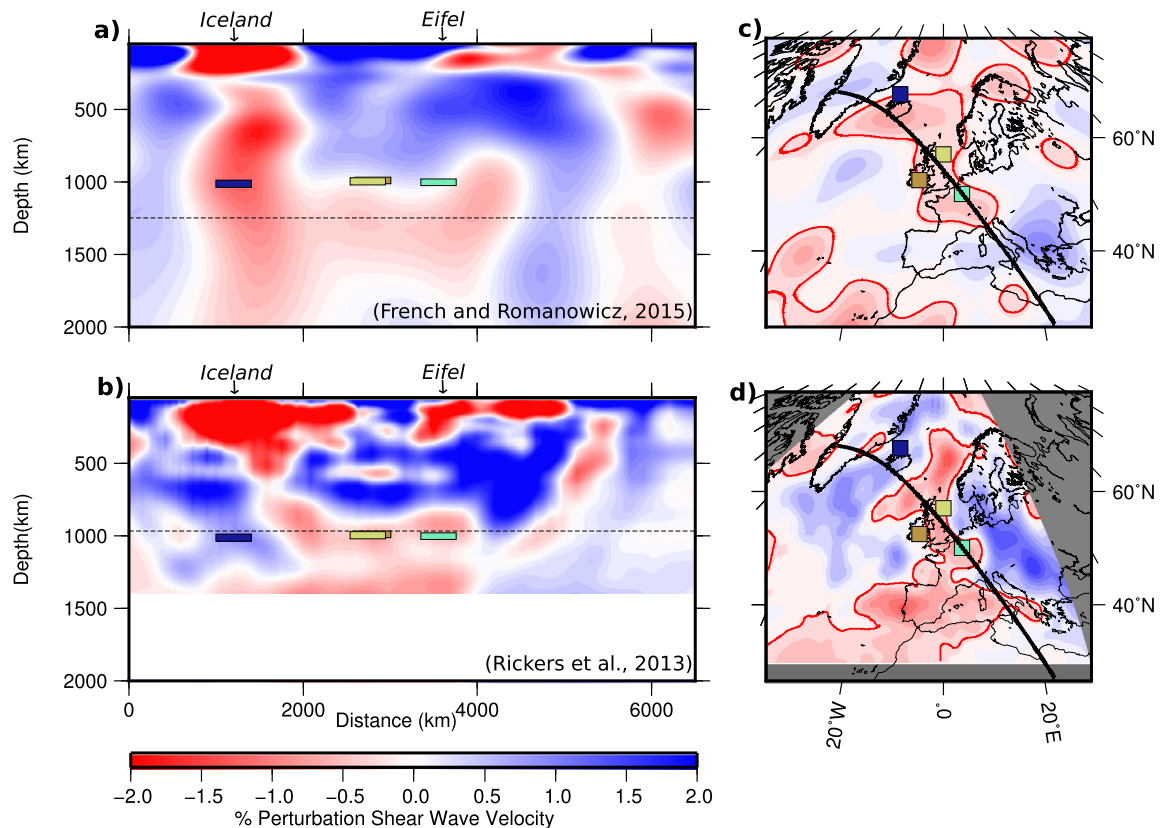
Fig. 10. Cross sections and depth slices through two recent tomographic models showing shear wave velocity variation: **a**) and **c**) French and Romanowicz (2015) and **b**) and **d**) Rickers et al. (2013). **c**) and **d**) show depth slices through the centre of elongate mid-mantle low velocity anomalies in the two models depths of 1250 km and 970 km respectively as indicated on the corresponding cross-section by dashed lines. The location of cross-sections is indicated on maps as a solid black line. Plotted on top of all sub-figures are locations where P1000s conversions are observed in regional stacks. Greyed out regions in **d**) represent poorly resolved areas at the edges of the station distribution used to create the regional north Atlantic model of Rickers et al. (2013).

4.2. Comparison to tomography – potential association with upwelling plume material

The recent shear wave velocity model of French and Romanow-icz (2015) shows a continuous low-velocity anomaly extending from the core mantle boundary to the Earth's surface beneath Iceland, which appears to be laterally diverted across Europe in the mid-mantle. This low-velocity feature correlates laterally and radially with our observations of mid-mantle discontinuities. Fig. 10 shows that the NW–SE trend of our clearest observations from the regional stacks are in fact coincident with the top of the laterally elongate low-velocity anomaly of French and Romanowicz (2015). A similar mid-mantle low-velocity anomaly is imaged by the regional North-Atlantic full waveform model of Rickers et al. (2013), although it is located roughly 200 km shallower. The difference in the depth of this feature between the two models, means that we are unable to conclude the exact location of our observations in relation to it. In the case of the French and Romanowicz (2015), the mapped discontinuities align with the top of the low-velocity feature, while in the case of Rickers et al. (2013), most of our mapped discontinuities lie within the low-velocity feature.

To create positive polarity arrivals, as we observe, conversions would have to be generated by a positive velocity jump with depth. This is the reverse of the negative velocity jump found at the top of the imaged low-velocity anomaly, with which our observations appear to correlate in the model of French and Romanow-icz (2015) model. Additionally, the anomaly imaged in both models is weak (∼0.5%) with diffuse edges, in contrast with our observations which are best explained by a sharp boundary of at least 1–2.5% increase in velocity. However, it should be noted that in tomographic models sharp boundaries will appear smoothed and

amplitudes of anomalies are generally underestimated. Our observations do not appear to correlate with a smoothed increase in velocity jump in tomographic models. This suggests that the velocity jumps causing converted phases are either so localised that they are beneath the horizontal resolution of tomographic models, or the velocity jump is followed by a gradual decrease in velocity, which is beneath the vertical resolution of tomographic models. While we cannot correlate the observed velocity jumps directly with the top or bottom of the low-velocity zones in the tomographic models, we can conclude that the observed discontinuities generally correlate with anomalously slow background material, potentially related to a diverted upwelling plume. This is different from most previous observations, which have been argued to correlate with high velocity anomalies related to active subduction zones nearby (see Fig. 1), but is consistent with a number of observations of mid-mantle seismic discontinuities seen in other areas of active upwelling (Shen et al., 2003; Le Stunff et al., 1995; Gu et al., 2009). In the next section, we will discuss interpretations in light of this potential correlation with upwelling plume material.

4.3. European mid-mantle discontinuities – potential interpretations

4.3.1. Temperature anomalies

One potential interpretation as to the underlying cause of the seismic velocity jump forming mid-mantle converted phases, is a thermal gradient. However explaining the observed conversions by a purely thermal gradient is unlikely based on the amplitude and sharpness of the related velocity jump.

Amplitudes of the observed P1000s conversions range from 0.8–2% of direct P arrival in the best regional stacks. This re-

quires a shear wave velocity increase of 1–2.5%, while frequency analysis indicates the increase occurs over a sharp transition of <8 km. The sensitivity of shear wave velocity (Vs) to temperature for a pyrolitic mantle around 1000 km depth is roughly -3.5×10^{-4} km s^{-1} K^{-1} (Cottaar et al., 2014). Given our minimum required shear wave velocity increase of 2.5% or 0.16 km s^{-1}, this requires a minimum temperature jump of -450 K, or thermal gradient of at least -57 K km^{-1} over 8 km, which is unrealistically high.

In addition to this, given the wide areas and number of RFs included in our regional stacks, observed amplitudes are likely to represent very conservative minimum estimates of the true arrival amplitude, as discussed in section 3.5. Indeed stacks within the smaller 2 degree caps show good arrivals with amplitudes of up to 4%, which would require an even higher temperature gradient if conversions were to be explained thermally. Thus we conclude that a thermal boundary layer cannot be considered as a viable cause of our observations. Sharp seismic velocity jumps are more generally explained by phase transitions or compositional layering, two cases we will explore below.

4.3.2. Phase transitions

The large peak seen by previous observations at ∼1000 km depth and the consistent ∼1000 km depth of conversions observed in the best multicap stacks in this study, suggest that a mineral phase change might occur at around this depth. Additionally, our synthetics show our observations can be explained by a single positive velocity jump. However, the non-continuous nature of observations and clear null regions indicate that this cannot be a global seismic discontinuity. Indeed there is no known phase change in a normal pyrolitic mantle composition that would explain the presence of mid-mantle seismic discontinuities (Murakami et al., 2005; Ono et al., 2005). So if we are to accept the hypothesis of a phase transition as the cause of our mid-mantle seismic discontinuities we must also suggest a chemically distinct composition that the phase change occurs within. The obvious candidate for this compositional change is the diverted plume material that observations appear to be coincident with. If a phase transition were to occur within plume material itself we might expect to see continuous observations within the low-velocity zone. Fig. 5 shows that this is not observed, but since the major gaps between observations are in oceans (North-Atlantic south-east of Iceland and across the English Channel), it is difficult to say whether observations are truly non-continuous or the lack of data in these regions means we are unable to image arrivals clearly.

Previous studies have suggested the following phase transitions in compositionally distinct material:

- Phase transitions in dense hydrous magnesium silicates such as serpentine (Shieh et al., 1998). Or the resulting metasomatic processes related to water released during dense hydrous magnesium silicate dehydration reactions that could produce chemical layering (Ohtani et al., 2001).
- Structural phase changes in silicate calcium perovskite from tetragonal to cubic structure, at temperatures lower than the normal mantle geotherm, as found in recently subducted material (Stixrude et al., 2007).
- A post-stishovite phase transition from rutile to CaCl structure which is hypothesised to take place in subducted oceanic crustal material (e.g. Kingma et al., 1995; Nomura et al., 2010).

Most previous studies have focused on subduction zone settings and the majority of phase change explanations for mid-mantle reflectors relate to mineralogies found in mid ocean ridge basalt (MORB) material. Accordingly, many of these interpretations are no longer viable outside areas of active subduction. However, the post-stishovite phase could occur in transported basaltic material, i.e. recycled oceanic crust, as also suggested by Vinnik et al. (2010). Stishovite, which would normally break down to form silicate perovskite, has been hypothesised to be preserved on the order of 100s Myrs (Bina, 2010), due to the formation of a perovskite reaction rims allowing subducted crustal material to survive as armoured relics. In pure stishovite it is thought that the phase change to post-stishovite occurs at approximately 1600 km depth (Nomura et al., 2010). However, recent studies which include small weight % oxides show that this depth is greatly reduced for more naturally realistic compositions, to depths of 900–1400 km dependent on the weight % of oxides (Lakshtanov et al., 2007). So, the post-stishovite phase transition might be able to explain our observations.

4.3.3. Small-scale chemical heterogeneity

Though the majority of our observations peak at 1000 km depth, we see a range of observations distributed throughout the investigated depth range of 800–1400 km. The non-continuous nature of the observed linear trend could be a real feature, as opposed to due to gaps in data coverage. Both of these facts argue for conversions that are generated by small scale patches of distributed chemically distinct material, whereas the correlation with slow velocities and potentially diverted mantle plume material could provide a source of entrained chemically distinct material.

One potential source of chemical heterogeneity is from remnants of recycled basaltic crustal material mixed throughout the mantle via convective processes. The increased density of basaltic compared to pyrolytic material is likely to cause it to sink into the lowermost mantle where it may accumulate. Many previous studies which have focused on subduction zone regions conclude that observations may represent fragments of subducted basaltic crust (e.g. Yang and He, 2015). While chemical diffusion processes are negligible, such material can be taken down into the lowermost mantle and brought back up in plumes while remaining compositionally distinct. This would suggest that our mid-mantle seismic observations could have the same cause as those observed in subduction zones, and explains why such features are seen in both regions of active downwelling and upwelling.

Alternatively, the mid-mantle seismic signals observed in subduction zones and associated with areas of upwelling, may not have the same underlying cause. The alternative to chemical heterogeneity sourced from above, is a source from below, such as a compositionally distinct deep mantle reservoir, which is sampled by upwelling plumes. Some studies have hypothesised that large low-shear-velocity provinces (LLSVPs) on the core–mantle boundary may be formed of primordial material from the remnants of an early magma ocean (Labrosse et al., 2007). Plumes which appear to rise from around the edges of LLSVPs (Burke et al., 2008) would be expected to entrain some of this potentially denser chemically distinct material (Kumagai et al., 2008). To complete this interpretation though, a mechanism of concentrating heterogeneity preferentially close to 1000 km depth is required. Compositional heterogeneity could pond around this depth if there were a viscosity jump (Marquardt and Miyagi, 2015; Rudolph et al., 2015), or if there were a neutral buoyancy crossover, e.g. for basaltic material (Ballmer et al., 2015), or for LLSVP-entrained-material (Kumagai et al., 2008). One complication comes from the observation that our most robust converted phases consist of a single positive pulse (Figs. 6 and 8) which can be explained by a single positive velocity jump. A scenario of un-mixed small-scale heterogeneities, or even a single thin layer of anomalous velocity, causes a more complex arrival with at least one negative pulse.

While we cannot give the final word on the observed seismic discontinuities being due to a local phase transition or to small-

scale chemical heterogeneity, we can state that either scenario requires a region that is compositionally distinct from the rest of the mid-mantle beneath Europe. Like all compositional variations in the lower mantle, the question remains if this heterogeneity is introduced over time through subduction (e.g. Christensen and Hofmann, 1994), has a primordial origin due to basal magma crystallisation (e.g., Labrosse et al., 2007), or a combination of both. Further study of mid-mantle discontinuities and their causes could shed light on the composition and dynamics of the mid-mantle region.

5. Conclusions

Using P-to-s RFs we map out mid-mantle seismic velocity jumps in a systematic continental wide study beneath Europe and the North-Atlantic. We make the following observations:

- Converted arrivals are distributed throughout the searched depth range of 800–1400 km but are dominated by positive amplitude observations from 1000 km depth.
- Arrival amplitudes vary from 0.8 to 4% of the direct P wave, indicative of a causative shear wave velocity increase with depth of 1 to 4%, while frequency analysis suggests this is a sharp transition happening over <8 km.
- The most robust observations show consistent depths of ~1000 km depth following a linear trend across Western Europe from Iceland in the northwest to Eifel in the southeast. They are coincident with areas of active upwelling (under Iceland) and an elongate lateral low velocity anomaly imaged in recent tomographic models and interpreted as diverted plume material at depth (Rickers et al., 2013; French and Romanowicz, 2015).

The lack of any phase change in a normal pyrolitic mantle composition at these depths indicates the presence of regional chemical heterogeneity within the mid-mantle, which is potentially caused by diverted plume material. We hypothesise observations may represent either a phase change within chemically distinct plume material itself, or small scale chemical heterogeneities entrained within the upwelling plume, either in the form of recycled basaltic material or deep sourced, chemically distinct material from LLSVPs. Our observations, which cannot be directly linked to an area of either active or ancient subduction, along with those made in other hotspot regions (Shen et al., 2003; Le Stunff et al., 1995; Gu et al., 2009), suggest that such mid-mantle seismic features are not unique to subduction zones despite the large number of observations that have previously been made in such settings.

Though the exact cause of such observations is not yet known, it is clear that it is no longer appropriate to think of the mid-mantle as the uniform homogeneous section between the interesting heterogeneous regions of the upper mantle and D″. Further large scale searches for observations of converted phases from mid-mantle heterogeneity will aid in defining if such features are truly associated only with areas of active upwelling and downwelling as they currently appear, or if they are a global if non-continuous feature. Further study on potential causes is required to draw conclusions on the composition and dynamics of the mid-mantle.

Acknowledgements

Appendix A. Supplementary material

Supplementary material related to this article can be found online at http://dx.doi.org/10.1016/j.epsl.2016.11.031.

References

An, Y., Gu, Y.J., Sacchi, M.D., 2007. Imaging mantle discontinuities using least squares radon transform. J. Geophys. Res., Solid Earth 112 (B10).

Ballmer, M.D., Schmerr, N.C., Nakagawa, T., Ritsema, J., 2015. Compositional mantle layering revealed by slab stagnation at ~1000-km depth. Sci. Adv. 1 (11), e1500815.

Bina, C.R., 2010. Scale limits of free-silica seismic scatterers in the lower mantle. Phys. Earth Planet. Inter. 183 (1), 110–114.

Bostock, M., 1999. Seismic waves converted from velocity gradient anomalies in the Earth's upper mantle. Geophys. J. Int. 138 (3), 747–756.

Burke, K., Steinberger, B., Torsvik, T.H., Smethurst, M.A., 2008. Plume generation zones at the margins of large low shear velocity provinces on the core–mantle boundary. Earth Planet. Sci. Lett. 265 (1), 49–60.

Castle, J.C., Van Der Hilst, R.D., 2003. Searching for seismic scattering off mantle interfaces between 800 km and 2000 km depth. J. Geophys. Res., Solid Earth 108 (B2).

Christensen, U.R., Hofmann, A.W., 1994. Segregation of subducted oceanic crust in the convecting mantle. J. Geophys. Res., Solid Earth 99 (B10), 19867–19884.

Cottaar, S., Deuss, A., 2016. Large-scale mantle discontinuity topography beneath Europe: signature of akimotoite in subducting slabs. J. Geophys. Res., Solid Earth 121 (1), 279–292.

Cottaar, S., Heister, T., Rose, I., Unterborn, C., 2014. Burnman: a lower mantle mineral physics toolkit. Geochem. Geophys. Geosyst. 15 (4), 1164–1179.

Courtier, A.M., Revenaugh, J., 2008. Slabs and shear wave reflectors in the midmantle. J. Geophys. Res., Solid Earth 113 (B8).

Deuss, A., 2009. Global observations of mantle discontinuities using SS and PP precursors. Surv. Geophys. 30 (4–5), 301–326.

Deuss, A., Andrews, J., Day, E., 2013. Seismic observations of mantle discontinuities and their mineralogical and dynamical interpretation. In: Physics and Chemistry of the Deep Earth, pp. 295–323.

Deuss, A., Woodhouse, J.H., 2002. A systematic search for mantle discontinuities using SS-precursors. Geophys. Res. Lett. 29 (8), 90–91.

Dziewonski, A.M., Anderson, D.L., 1981. Preliminary reference Earth model. Phys. Earth Planet. Inter. 25 (4), 297–356.

French, S.W., Romanowicz, B., 2015. Broad plumes rooted at the base of the Earth's mantle beneath major hotspots. Nature 525 (7567), 95–99.

Fuchs, K., Müller, G., 1971. Computation of synthetic seismograms with the reflectivity method and comparison with observations. Geophys. J. Int. 23 (4), 417–433.

Fukao, Y., Obayashi, M., 2013. Subducted slabs stagnant above, penetrating through, and trapped below the 660 km discontinuity. J. Geophys. Res., Solid Earth 118 (11), 5920–5938.

Gu, Y.J., An, Y., Sacchi, M., Schultz, R., Ritsema, J., 2009. Mantle reflectivity structure beneath oceanic hotspots. Geophys. J. Int. 178 (3), 1456–1472.

Jenkins, J., Cottaar, S., White, R., Deuss, A., 2016. Depressed mantle discontinuities beneath Iceland: evidence of a garnet controlled 660 km discontinuity? Earth Planet. Sci. Lett. 433, 159–168.

Kaneshima, S., 2016. Seismic scatterers in the mid-lower mantle. Phys. Earth Planet. Inter. 257, 105–114.

Kaneshima, S., Helffrich, G., 1999. Dipping low-velocity layer in the mid-lower mantle: evidence for geochemical heterogeneity. Science 283 (5409), 1888–1892.

Kawakatsu, H., Niu, F., et al., 1994. Seismic evidence for a 920-km discontinuity in the mantle. Nature 371 (6495), 301–305.

Kingma, K.J., Cohen, R.E., Hemley, R.J., Mao, H.-K., et al., 1995. Transformation of stishovite to a denser phase at lower-mantle pressures. Nature 374 (6519), 243–245.

Kumagai, I., Davaille, A., Kurita, K., Stutzmann, E., 2008. Mantle plumes: thin, fat, successful, or failing? Constraints to explain hot spot volcanism through time and space. Geophys. Res. Lett. 35 (16).

Labrosse, S., Hernlund, J., Coltice, N., 2007. A crystallizing dense magma ocean at the base of the Earth's mantle. Nature 450 (7171), 866–869.

Lakshtanov, D.L., Sinogeikin, S.V., Litasov, K.D., Prakapenka, V.B., Hellwig, H., Wang, J., Sanches-Valle, C., Perrillat, J.-P., Chen, B., Somayazulu, M., et al., 2007. The post-stishovite phase transition in hydrous alumina-bearing SiO_2 in the lower mantle of the Earth. Proc. Natl. Acad. Sci. 104 (34), 13588–13590.

Le Stunff, Y., Wicks Jr, C.W., Romanowicz, B., 1995. P'P' precursors under Africa: evidence for mid-mantle reflectors. Science 270 (5233), 74.

Ligorría, J.P., Ammon, C.J., 1999. Iterative deconvolution and receiver-function estimation. Bull. Seismol. Soc. Am. 89 (5), 1395–1400.

Marquardt, H., Miyagi, L., 2015. Slab stagnation in the shallow lower mantle linked to an increase in mantle viscosity. Nat. Geosci. 8 (4), 311–314.

Murakami, M., Hirose, K., Sata, N., Ohishi, Y., 2005. Post-perovskite phase transition and mineral chemistry in the pyrolitic lowermost mantle. Geophys. Res. Lett. 32 (3).

Nomura, R., Hirose, K., Sata, N., Ohishi, Y., 2010. Precise determination of post-stishovite phase transition boundary and implications for seismic heterogeneities in the mid-lower mantle. Phys. Earth Planet. Inter. 183 (1), 104–109.

Ohtani, E., Toma, M., Litasov, K., Kubo, T., Suzuki, A., 2001. Stability of dense hydrous magnesium silicate phases and water storage capacity in the transition zone and lower mantle. Phys. Earth Planet. Inter. 124 (1), 105–117.

Ono, S., Ohishi, Y., Isshiki, M., Watanuki, T., 2005. In situ X-ray observations of phase assemblages in peridotite and basalt compositions at lower mantle conditions: Implications for density of subducted oceanic plate. J. Geophys. Res., Solid Earth 110 (B2).

Rakhmanov, E.A., Saff, E., Zhou, Y., 1994. Minimal discrete energy on the sphere. Math. Res. Lett. 1 (6), 647–662.

Rickers, F., Fichtner, A., Trampert, J., 2013. The Iceland–Jan Mayen plume system and its impact on mantle dynamics in the North Atlantic region: evidence from full-waveform inversion. Earth Planet. Sci. Lett. 367, 39–51.

Ritsema, J., Deuss, A., Van Heijst, H., Woodhouse, J., 2011. S40RTS: a degree-40 shear-velocity model for the mantle from new Rayleigh wave dispersion, teleseismic traveltime and normal-mode splitting function measurements. Geophys. J. Int. 184 (3), 1223–1236.

Rost, S., Garnero, E.J., Williams, Q., 2008. Seismic array detection of subducted oceanic crust in the lower mantle. J. Geophys. Res., Solid Earth 113 (B6).

Rudolph, M.L., Lekić, V., Lithgow-Bertelloni, C., 2015. Viscosity jump in Earth's midmantle. Science 350 (6266), 1349–1352.

Schmandt, B., 2012. Mantle transition zone shear velocity gradients beneath US-Array. Earth Planet. Sci. Lett. 355, 119–130.

Shen, Y., Wolfe, C.J., Solomon, S.C., 2003. Seismological evidence for a mid-mantle discontinuity beneath Hawaii and Iceland. Earth Planet. Sci. Lett. 214 (1), 143–151.

Shieh, S.R., Mao, H.-k., Hemley, R.J., Ming, L.C., 1998. Decomposition of phase d in the lower mantle and the fate of dense hydrous silicates in subducting slabs. Earth Planet. Sci. Lett. 159 (1), 13–23.

Stixrude, L., Lithgow-Bertelloni, C., Kiefer, B., Fumagalli, P., 2007. Phase stability and shear softening in $CaSiO_3$ perovskite at high pressure. Phys. Rev. B 75 (2), 024108.

van der Meijde, M., Marone, F., Giardini, D., van der Lee, S., 2003. Seismic evidence for water deep in Earth's upper mantle. Science 300 (5625), 1556–1558.

Van der Meijde, M., Van der Lee, S., Giardini, D., 2005. Seismic discontinuities in the Mediterranean mantle. Phys. Earth Planet. Inter. 148 (2), 233–250.

Vanacore, E., Niu, F., Kawakatsu, H., 2006. Observations of the mid-mantle discontinuity beneath Indonesia from S to P converted waveforms. Geophys. Res. Lett. 33 (4).

Vinnik, L., Kato, M., Kawakatsu, H., 2001. Search for seismic discontinuities in the lower mantle. Geophys. J. Int. 147 (1), 41–56.

Vinnik, L., Oreshin, S., Speziale, S., Weber, M., 2010. Mid-mantle layering from SKS receiver functions. Geophys. Res. Lett. 37 (24).

Wessel, P., Smith, W.H., 2001. The Generic Mapping Tools.

Yang, Z., He, X., 2015. Oceanic crust in the mid-mantle beneath west-central Pacific subduction zones: evidence from S to P converted waveforms. Geophys. J. Int. 203 (1), 541–547.

Zhu, H., Bozdağ, E., Tromp, J., 2015. Seismic structure of the European upper mantle based on adjoint tomography. Geophys. J. Int. 201 (1), 18–52.